

Sharpness Functions for Computational Aesthetics and Image Sublimation

Maria Rudnaya, and Robert Ochshorn

Abstract—The goal of this paper is to establish a link between existing autofocus methodology and computational aesthetics. Many existing autofocus methods are based on a sharpness function, a real-valued estimate of the image’s sharpness. The intensity-based sharpness function has already been applied in computational aesthetics before. In this paper we apply a wider range of sharpness functions for aesthetics measurement in photographic images. Additionally, we use the full two-dimensional result of the sharpness function in a visualization technique we term “sublimation.”

Index Terms—image quality, image manipulation, sharpness function, photography, computational aesthetics, image sublimation

I. INTRODUCTION

AN image obtained with an optical device, such as a photcamera, a telescope or a microscope, depends on a given object’s geometry, known as the *object function*, and the optical device *control variables* (for instance, *defocus*). The method of automatic defocus determination, such that the recorded image is *in-focus*, is known as *autofocus* method. Many existing autofocus methods are based on a *sharpness function*, a real-valued estimate of the image’s sharpness.

Aesthetics is the branch of philosophy that deals with the nature and expression of beauty [1]. Certain visual properties, such as sharpness, contrast, light and colorfulness make a photograph more beautiful [2], [3]. A number of issues make the measurement of aesthetics in pictures or photographs extremely subjective. In [3] an example of an automated aesthetics measurement has been demonstrated for a large set of photographic images. In particular the aesthetics has been measured by pixel intensity average, which is known in autofocus applications as *intensity-based sharpness function*.

The goal of this paper is to establish a link between existing autofocus methodology and computational aesthetics. The sharpness functions we are applying for the aesthetics measurement are the generalized versions of the intensity-based sharpness function. In addition to gradient-based sharpness function investigated earlier in [4], we introduce the variance-based and the histogram-based sharpness functions. These functions are experimentally applied for the computations of aesthetics in photographic images. Two various applications within the field are considered, and a sublimation operation is defined and tested.

The paper is set up as follows: Section II describes the general image formation model. This model is used for

Manuscript received October 14, 2011; revised , 2011.

M. Rudnaya is with the Department of Mathematics and Computer Science, Eindhoven University of Technology, The Netherlands, e-mail: maria.rudnaya@gmail.com.

R. Ochshorn is with the Department of Design, Jan van Eyck Academy, Maastricht, The Netherlands, e-mail: mail@rmozone.com.

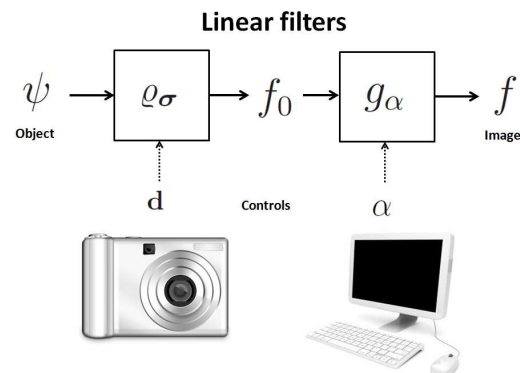


Fig. 1. The image formation model.

the sharpness function definition and analysis of their basic properties. Sections III, IV, V introduce derivative-based, variance-based and histogram-based sharpness functions correspondingly. Section VI presents the results of numerical experiments: in Subsection VI-A we use as experimental data the photographs collected from open websites with statistical system of quality evaluation; in Subsection VI-B photographs taken by one photographer within one photoshoot are used. Section VII defines the *sublimation* transformation, which enhances those sections of an image determined by the sharpness function to be important. Section VIII provides discussions and future recommendations.

II. MODELLING

In this section we provide a brief explanation of the model that has been used in the previous research on the autofocus methods [4], [5]. The Fourier transform \hat{f} of a function $f \in \mathcal{L}^2(\mathbb{R})$ is defined as follows

$$\hat{f}(\omega) = \int_{-\infty}^{\infty} f(x)e^{-i\omega x} dx,$$

where x is a *spatial coordinate* and ω is a *frequency coordinate*. The vector of spatial coordinates in two-dimensions is denoted by $\mathbf{x} := (x, y)^T \in \mathbb{R}^2$. For a vector $\mathbf{w} := (w_i)_{i=1}^N$ we define $\|\mathbf{w}\| := (\sum_i |w_i|^2)^{1/2}$. The L_p -norm of a function is defined as

$$\|f\|_{L_p} := \left(\int_{-\infty}^{\infty} |f|^p dx \right)^{1/p}, \quad p = 1, 2, 3, \dots$$

and $\mathbb{L}_p(\mathbb{R}^2)$ is the space of functions with finite L_p -norm.

A. Linear image formation model

Images for which our sharpness function will be computed are the output images $f \in \mathbb{L}_2(\mathbb{R}^2)$ of the so-called *image*

formation model represented by Figure 1. The object's geometry (or the *object function*) is denoted by ψ . The filter ϱ_σ describes the *point spread function* of an optical device.

The output of the ϱ_σ filter is denoted by f_0 and is often post-processed by a PC. We assume that in such post-processing a Gaussian filter $g_\alpha(\mathbf{x}) := \frac{1}{2\pi\alpha^2} e^{-\frac{\|\mathbf{x}\|^2}{2\alpha^2}}$ is applied to the image f_0 . Filtering with a Gaussian kernel is often used for denoising purposes, which is an easy alternative to more advanced techniques [6], [7], [8]. It has been shown that the control variable α is useful not only for denoising the image f_0 ; it also influences the approximation error when the sharpness function is replaced by a quadratic polynomial in an autofocus application [5].

We apply the *linear image formation model*, which is often used for different optical devices [9]. This implies that the occurring filters are linear and space invariant which can easily be described by means of *convolution* products

$$f_0 := \psi * \varrho_\sigma, \quad f := f_0 * g_\alpha. \quad (1)$$

If no post-processing is applied, $\alpha = 0$, and $f = f_0$.

The point spread function can accurately be approximated by a *Lévi stable density* function for a wide class of optical devices [10], [11]. The Lévi stable density function is implicitly defined via its Fourier transform in one-dimension as follows

$$\hat{\varrho}_\sigma(\omega) := e^{-\sigma^2 \omega^{2\beta}/2}, \quad 0 < \beta \leq 1. \quad (2)$$

The parameter β in (2) depends on the optical device. If $\beta = 1$ in (2), the point spread function is a Gaussian function. The parameter σ in (2) is known as the *width* of the point spread function and has a linear relation with the optical device defocus.

B. Discrete images

In real-world applications the image f is always camera-recorded, and therefore discrete and bounded. Assume for $X, Y \in \mathbb{R}$ the support of f is

$$\mathbb{X} := [0, X] \times [0, Y],$$

i.e., $f(\mathbf{x}) = 0$ for \mathbf{x} outside of \mathbb{X} . For $i = 1, \dots, N$, $j = 1, \dots, M$ and $\Delta x := \frac{X}{N}$, $\Delta y := \frac{Y}{M}$, we define the grid points

$$x_i := \frac{\Delta x}{2} + (i-1)\Delta x, \quad y_j := \frac{\Delta y}{2} + (j-1)\Delta y.$$

Thus for the default $X = Y = 1$, $\Delta x = \frac{1}{N}$, $\Delta y = \frac{1}{M}$. In practice Δx is often equal to Δy . The discrete images can be represented by a matrix

$$\mathbf{F} := (f_{i,j})_{i,j=1}^N, \quad (3)$$

of the *image pixel values*

$$f_{i,j} := f(x_i, y_j). \quad (4)$$

We use the *mid-point rule* for approximation of image integration. Hence the integration of the image with compact support over the image domain in two-dimension is approximated by

$$\int_{\mathbb{X}} f(\mathbf{x}) d\mathbf{x} \doteq \Delta x \Delta y \sum_{i,j} f(x_i, y_j)$$

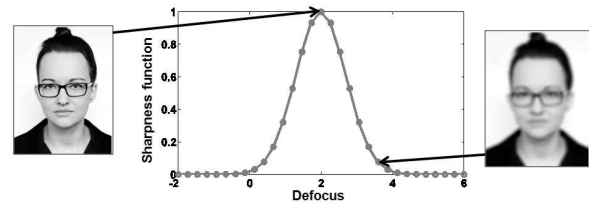


Fig. 2. Sharpness function reaches its optimum at the in-focus image. The goal of the autofocus procedure is to find the value of the defocus.

$$\doteq \frac{1}{NM} \sum_{i,j=1}^{N,M} f_{i,j}, \quad (5)$$

similarly

$$\|f\|_{L_p} \doteq \left(\frac{1}{NM} \sum_{i,j=1}^{N,M} f_{i,j}^p \right)^{1/p}.$$

For the given discrete image the sampling periods Δx , Δy are fixed. Thus considering higher order integration will not decrease the integration error.

Below we discuss the numerical differentiation of the discrete images. By dropping the limit in the definition of the *differential operator*

$$\frac{\partial}{\partial x} f(\mathbf{x}) := \lim_{\epsilon \rightarrow 0} \frac{f(x + \epsilon, y) - f(x, y)}{\epsilon}$$

and keeping ϵ fixed at a distance of $k \in \mathbb{N}$ pixels, we obtain a *finite difference* approximation at (x_i, y_j)

$$\frac{\partial}{\partial x} f(x_i, y_j) \doteq \frac{1}{(k\Delta x)} (f_{i+k,j} - f_{i,j}). \quad (6)$$

We refer to k as the *pixel difference* parameter for the discrete image derivatives.

Two alternative derivative interpolation solutions appear commonly in the literature: fitting polynomial approximations [12] and smoothing with a filter, for instance a Gaussian function [13]

$$\frac{\partial}{\partial x} f(\mathbf{x}) \doteq \mathcal{D}_x := \frac{\partial}{\partial x} (f * g) = f * \frac{\partial}{\partial x} g. \quad (7)$$

C. Sharpness functions

Many existing *autofocus* methods are based on a *sharpness function* $S : \mathbb{L}_2(\mathbb{R}^2) \rightarrow \mathbb{R}$, a real-valued estimate of the image's sharpness. In the literature a number of sharpness functions have been considered and discussed for different optical devices, such as photographic and video cameras [14], [15], telescopes [16] and microscopes [17], [18], [19]. In autofocus application for a *through-focus series* of images the sharpness function is computed for different values of d given a fixed value of α . A typical sharpness function shape application is shown in Figure 2. The image at the ideal defocus values is sharp or *in-focus* when the sharpness function reaches its optimum. An image away from the ideal defocus value is called *out-of-focus*. An *ideal sharpness functions* should have a single optimum (maximum or minimum) at the in-focus image. The sharpness functions are also used for other studies, for instance the *hysteresis* in electromagnetic lenses [20] and reconstructions of three-dimensional microscopic objects [8], [9].

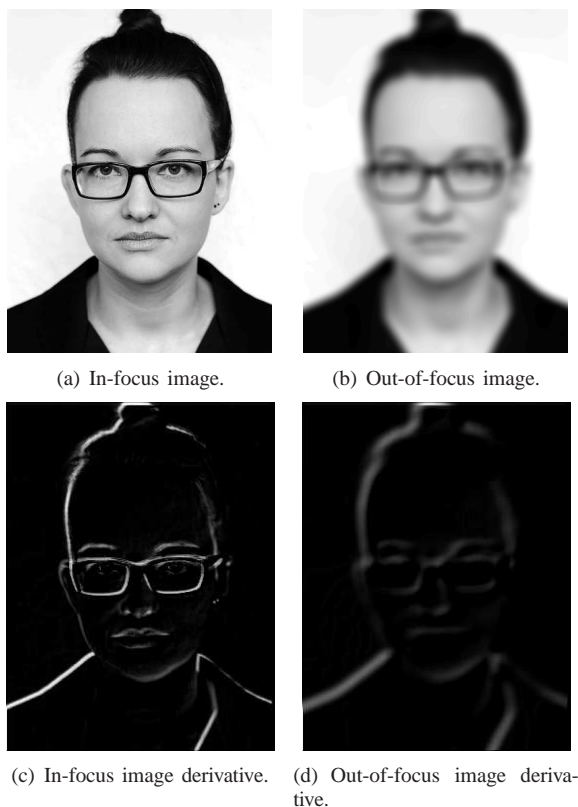


Fig. 3. In-focus and out-of-focus images, and their derivatives.

For the aesthetics study in photographic images in [3] within a set of methods the intensity-based sharpness function is applied

$$S^{\text{int}}[f] := \|f\|_{L_2}^2. \quad (8)$$

In this paper we consider an extended family of sharpness functions for the computational aesthetics study.

III. DERIVATIVE-BASED SHARPNESS FUNCTION

The advantage of using derivative-based sharpness functions has been shown experimentally for various optical devices [9], [18], [19], [21]. The use of these functions used to be heuristic. Usually they are based on the assumption that the *in-focus* image has a larger difference between neighbouring *pixels* than the *out-of-focus* image. Figure 3 shows in-focus and out-of-focus images and their numerically computed derivatives, which are images as well. We can observe that the derivative of the in-focus image (Figure 3(c)) has stronger intensity (higher pixel values) than the derivative of the out-of-focus image (Figure 3(d)).

The derivative-based sharpness function is defined (cf.[15], [21])

$$S[f] := \left\| \frac{\partial^n}{\partial x^n} f \right\|_{L_p}^p, \quad n \in \mathbb{Z}^+, \quad p = 1, 2. \quad (9)$$

For $n = 0$ in (9) we obtain the intensity-based sharpness function (8). In different literature sources different norms are applied to the image derivatives for autofocus purposes, i.e. $p = 1$ in [22], [23] or $p = 2$ in [14], [16]. We mostly focus on $p = 2$ in (9). It will be explained below that L_2 -norm derivative-based sharpness functions are less sensitive to *noise* than L_1 -norm based. For the linear image formation

model (1), we have therefore

$$S = \left\| \frac{\partial^n}{\partial x^n} (\psi * \varrho_\sigma * g_\alpha) \right\|_{L_2}^2. \quad (10)$$

Property 1. *The sharpness function (10) can be expressed as follows*

$$S(\sigma) = \frac{1}{2\pi} \int_{-\infty}^{\infty} \omega^{2n} |\hat{\psi}(\omega)|^2 e^{-\sigma^{2\beta} \omega^{2\beta}} e^{-\alpha^2 \omega^2} d\omega. \quad (11)$$

Proof: For $\hat{\psi}, \hat{g}, \hat{f}$, the Fourier transforms of ψ, g, f respectively, it holds that $\hat{f} = \hat{\psi} \hat{\varrho}_\sigma \hat{g}_\alpha$. Then from *Parseval's identity* we find

$$\begin{aligned} S(\sigma) &= \left\| \frac{\partial^n}{\partial x^n} f \right\|_{L_2}^2 = \frac{1}{2\pi} \|\omega^n \hat{f}\|_{L_2}^2 = \\ &= \frac{1}{2\pi} \int_{-\infty}^{\infty} \omega^{2n} |\hat{\psi}(\omega)|^2 |\hat{\varrho}_\sigma(\omega)|^2 |\hat{g}_\alpha(\omega)|^2 d\omega. \end{aligned}$$

Property 1 is a generalized version of the property that has been demonstrated before in [5]. The following corollaries follow directly from Property 1.

Corollary 1. *The sharpness function (10) is smooth, and is strictly increasing for $\sigma < 0$ and strictly decreasing for $\sigma > 0$.*

Corollary 2. *For $\alpha > 0$ the sharpness function (10) has a finite maximum at $\sigma = 0$*

$$\max_{\sigma} S(\sigma) = S(0).$$

The property and corollaries described above are very important for autofocus problem. They show that for the suggested model with the noise-free image formation the function (9) satisfies the properties of the *ideal sharpness function*. It is important to note that in computational aesthetics the situation is more difficult because we would mostly deal with the images recorded from recorded using different object functions ψ . Moreover, even the amount of pixels in the discrete images we are going to compare can appear to be different. To deal with such situations in a proper way a careful discretization of the sharpness functions is required.

A. Sharpness function discretization

In this paper we pay a special attention to the proper discretization of the sharpness functions (especially derivative-based sharpness function), which has not been done in the previous work [4], [5]. The proper normalization coefficient in front of the discrete sharpness function is important if we compare the sharpness function values of images with different geometries.

It trivially follows from (6) that for the default $\Delta x = 1/N$

$$\left(\frac{\partial}{\partial x} f(x_i, y_j) \right)^p \doteq \frac{1}{k^p N^{1-p}} (f_{i+k, j} - f_{i, j})^p. \quad (12)$$

Using discrete integration (5), we obtain a discrete version of the sharpness function (9) for $n = 1$

$$S \doteq s_x^{\text{der}} := \frac{1}{k^p N^{1-p} M} \sum_{i, j} |f_{i, j} - f_{i, j+k}|^p, \quad (13)$$

where k (the *pixel difference*) adjusts the sensitivity of the sharpness function to the noisy images. It is clear that for $n = 2$ in (13) larger differences between pixels are weighted more strongly than smaller ones. This leads to the suppression of the contribution made by noise [24]. To improve the robustness to noise a threshold Θ is often applied to the difference between pixels, which is taken into account [23]

$$s_{x,\Theta}^{\text{der}} := \frac{1}{N^{1-p} M k^p} \sum_{i,j} |f_{i,j} - f_{i,j+k}|^p, \quad (14)$$

$$|f_{i,j} - f_{i,j+k}|^p > \Theta, \quad \Theta > 0.$$

The threshold Θ is determined experimentally [24]. In scanning electron microscopes often the difference between only the pixels in horizontal direction is taken into account, because the scanning is performed in horizontal direction and therefore noise is correlated there. This sharpness function can fail for certain image geometries (for example, a number or uniform horizontal stripes). Let $s_{y,\Theta}^{\text{der}}$ be the function that computes the norm of the pixel difference in vertical direction. Then the form that generalizes derivative-based sharpness function is

$$s_{\Theta}^{\text{der,c}} := s_{x,\Theta}^{\text{der}} + \nu s_{y,\Theta}^{\text{der}}, \quad \nu = \{0, 1\}. \quad (15)$$

Usually in applications only pixel difference parameter values $k = 1, 2$ are used [21], [25]. However, it has been experimentally shown that in some applications the larger values of k often provide better results [19].

If we consider derivative interpolation by a convolution with a Gaussian derivative kernel (7), we obtain

$$s_{\Theta}^{\text{der,c}} = \sum_{i,j} \left((\mathbf{F} * \mathbf{G}_1)_{i,j}^2 + (\mathbf{F} * \mathbf{G}_2)_{i,j}^2 \right), \quad (16)$$

$$\left((\mathbf{F} * \mathbf{G}_1)_{i,j}^2 + (\mathbf{F} * \mathbf{G}_2)_{i,j}^2 \right) > \Theta,$$

where the Gaussian derivative kernels $\mathbf{G}_1, \mathbf{G}_2$ could be for instance defined as

$$\mathbf{G}_1 = \begin{pmatrix} -1 & 0 & 1 \\ -2 & 0 & 2 \\ -1 & 0 & 1 \end{pmatrix}, \quad \mathbf{G}_2 = \begin{pmatrix} 1 & 2 & 1 \\ 0 & 0 & 0 \\ -1 & -2 & -1 \end{pmatrix}. \quad (17)$$

The form of Gaussian kernels (17) is known in application literature as *Sobel operators* [25]. For the model explained in the previous section as shown in (7) such an approach could already include the value of the blur parameter α .

IV. VARIANCE-BASED SHARPNESS FUNCTION

For an image f with compact support \mathbb{X} , its mean value $E[f]$ is defined as

$$E[f] := \bar{f} := \left(\iint_{\mathbb{X}} f \, d\mathbf{x} \right) / \left(\iint_{\mathbb{X}} d\mathbf{x} \right) \quad (18)$$

The variance-based sharpness function is defined as (cf. [26], [27])

$$S^{\text{var}}[f] := \|f - \bar{f}\|_{L_2}^2. \quad (19)$$

Consider the amplitude image function

$$f^{(A)} := f - \bar{f}.$$

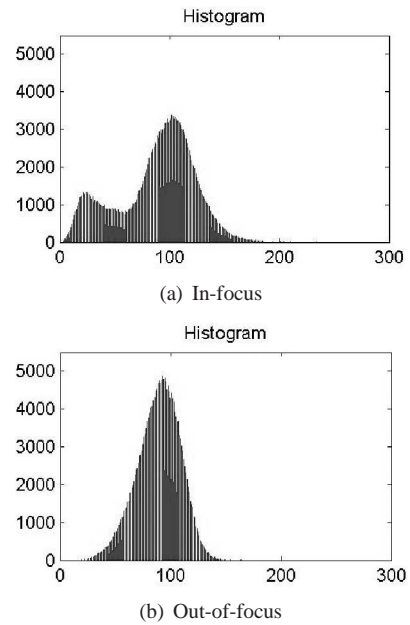


Fig. 4. Histograms computed for in-focus and out-of-focus experimental images of the same object.

It follows from the definition that the mean value of the image amplitude function is equal to zero

$$E[f^{(A)}] = \left(\iint_{\mathbb{X}} f \, d\mathbf{x} - \bar{f} \iint_{\mathbb{X}} d\mathbf{x} \right) / \left(\iint_{\mathbb{X}} d\mathbf{x} \right) = 0.$$

In some applications the amplitude image function $f^{(A)}$ is used instead of f for the sharpness analysis (cf. [26]). In this case we obtain $S^{\text{var}}[f^{(A)}] = S^{\text{var}}[f - \bar{f}] = \|f\|_{L_2}^2$, which is known as the intensity-based sharpness function (8).

For the discrete image the mean value is approximated by

$$\bar{f} \doteq \bar{F} := \frac{\sum_{i,j} \Delta x^2 f_{i,j}}{\sum_{i,j} \Delta x^2} = \frac{1}{N^2} \sum_{i,j} f_{i,j} \quad (20)$$

and the discrete variance-based sharpness function is

$$S^{\text{var}} \doteq s^{\text{var}} := \frac{1}{N^2} \sum_{i,j} (f_{i,j} - \bar{F})^2. \quad (21)$$

V. HISTOGRAM-BASED SHARPNESS FUNCTION

Histograms are often used as a basis for the image quality measurement in computational aesthetics [28], as well as in image enhancement [29]. The histogram-based sharpness function is defined in the discrete space only, because it deals directly with the image pixel values. In most applications the unscaled image \mathbf{F} is a matrix of natural intensity values. Let

$$\tilde{\mathbf{f}} = (\tilde{f}_k)_{k=1}^L, \quad \tilde{f}_{k-1} < \tilde{f}_k,$$

be a set of all pixel values in the image \mathbf{F} , i.e. $f_{i,j} \in \mathbf{F} \Leftrightarrow \exists k$ such that $f_{i,j} = \tilde{f}_k \in \tilde{\mathbf{f}}$. The vector $\mathbf{h} = (h_k)_{k=1}^L$, where h_k is the number of pixels with the value \tilde{f}_k in the image \mathbf{F} , is called the *histogram* of the image \mathbf{F} . Then the probability of a pixel value equal to \tilde{f}_k is $\frac{h_k}{N^2}$.

Figure 4 shows the histograms of in-focus and out-of-focus experimental images. The horizontal axis on each diagram represents the pixel gray values, and the vertical axis the number of counts \mathbf{h} . The in-focus image has the whole range of the pixel values, including pixels equal to 0 and to 255.



Fig. 5. A typical landscape colored photo with the straight horizon line.

The out-of-focus image has less contrast, and its values in this case are spread between 12 and 130. These observations lead to the histogram-based sharpness function, known as histogram range [25]

$$S^{\text{his}_r} := \max_{k, h_k \neq 0} h_k - \min_{k, h_k \neq 0} h_k. \quad (22)$$

It is clear from the above example that the larger the range the more contrast the image has, and the more information it contains. Other histogram-based sharpness functions are the entropy (cf. [30])

$$S^{\text{his}_e} := - \sum_{k, h_k \neq 0} \frac{h_k}{N^2} \log_2 \frac{h_k}{N^2}. \quad (23)$$

and the threshold image count (cf. [25])

$$S^{\text{his}_t} := \sum_{k=1}^n h_k, \quad \tilde{f}_n \leq \Theta \quad \tilde{f}_{n+1} > \Theta. \quad (24)$$

VI. SHARPNESS FUNCTIONS FOR COMPUTATIONAL AESTHETICS

In this section two experiments with the real-world data are described. In Subsection VI-A sharpness functions are applied to a number of photographs that have been downloaded from a photography website. The results are compared with the scores given to the same photographs by the users of the website. In Subsection VI-B various sharpness functions are applied to the photographs taken within the same setting. The results provide the possible indication and assistance for a human user in the choice of a better quality picture recorded within one session.

A. Various settings

The photography websites, such as flickr.com, photo.net, photosight.ru usually have an assessment system for the quality evaluation of the manual photographs. The total score that can be obtained by one photo within such a system consist of a few factors. First of all the users can indicate if they like the photo and add it to the list of their favorites. Usually the most interesting images receive the highest amount of views. Also, the most interesting photos often receive a large amount of comments. Thus, the total score which is suggested to compute for one photo is

$$z_{\text{tot}} = z_{\text{view}} + 10 * z_{\text{like}} + 20 * z_{\text{fav}} + 5 * z_{\text{comm}}, \quad (25)$$

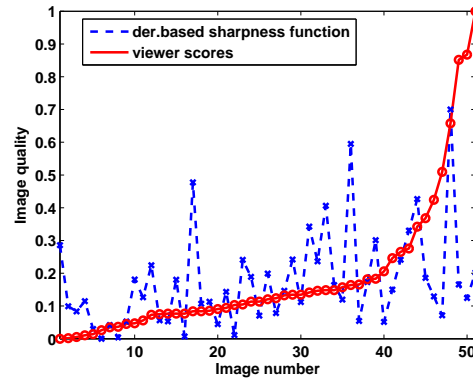


Fig. 6. Experiments with derivative-based sharpness function and experimental data from a photography website.

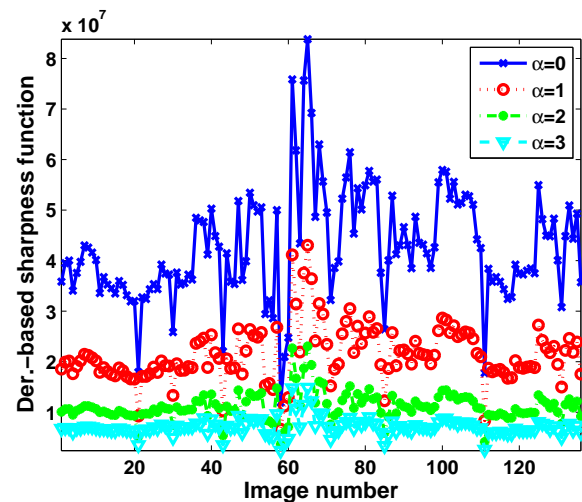


Fig. 9. Derivative-based sharpness function computed for experimental data for different values of α .

where z_{view} is the amount of views the photo received, z_{like} is the amount of people that indicated they like the photo, z_{fav} is the amount of people that have added the photo to their favorite list, and z_{comm} is the amount of comments that the photo received.

A number of colorful photographs of the landscapes have been downloaded from a photography website. An example of a typical landscape is shown in Figure 6. Each of the landscape has the straight horizon line. The photographs did not have any object created by human on them. Each of the photographs have been uploaded to the website within two days more than one month before our experiment took place. All collected photos are made by photographers of approximately the same level (they are registered on the website as amateurs, not as professionals).

In our practical experiment we deal with colorful photographs. It implies that each photograph consists of three images (three two-dimensional matrixes) which are presented as one picture via so-called RGB space [31]. In photography and color psychology color tones and saturation play important role, and hence working in HSV color space makes computations more convenient. As well as in [3] we convert the photographs from RGB to HSV color space, which results in three discrete images $\mathbf{F}_H, \mathbf{F}_S, \mathbf{F}_V$. For every photograph the discrete derivative-based sharpness function $s^{\text{der}}[\mathbf{F}_S]$ is

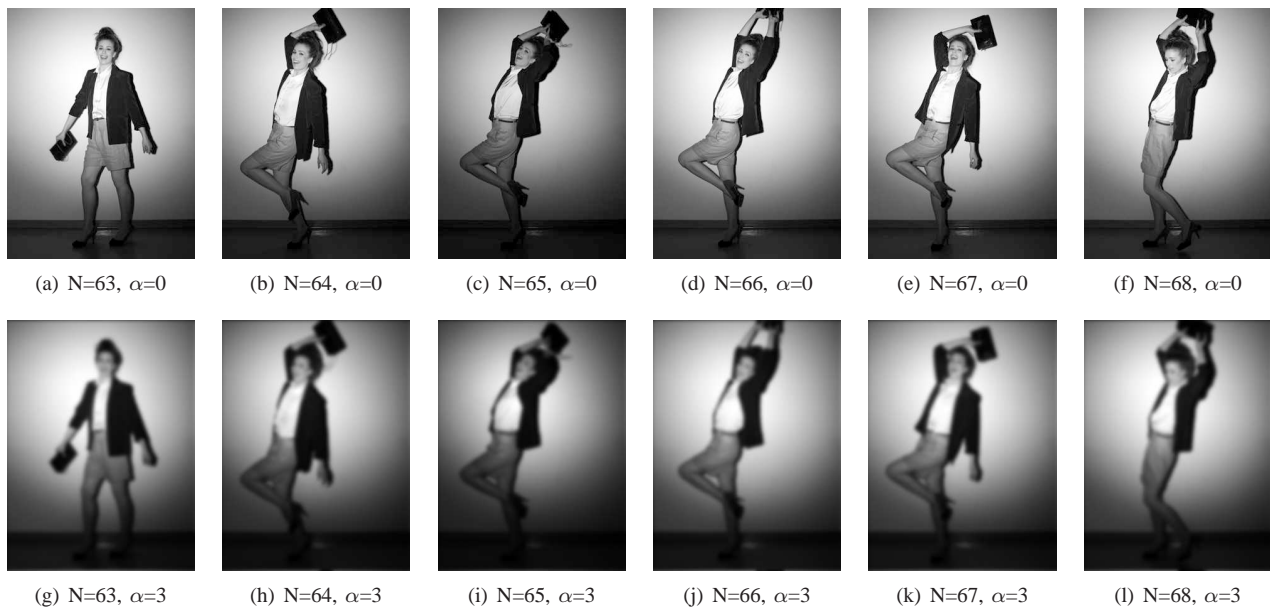


Fig. 7. Experimental photography data: upper row, $\alpha = 0$, lower row, $\alpha = 3$.

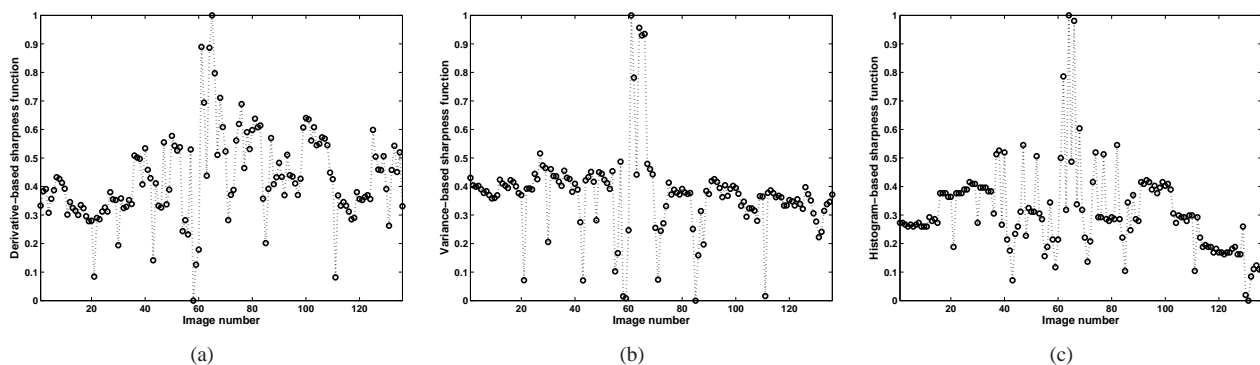


Fig. 8. Sharpness functions computed for experimental data.

computed. Next to it for every photograph the total quality score is computed with (25) based on the statistical data collected from the website.

Figure 6 shows the normalized scores and the values of derivative-based sharpness function computed for 51 experimental photographs. Let s be the vector of sharpness function values and z be the vector of the computed scores for the given set of images. The computed *least square difference* between the data sets is 23 %, i.e. $\|s - z\|_{l_2} = 0.23$. Similar results are obtained for the sharpness function $s^{\text{der}}[\mathbf{F}_V]$. Though, the results are diverse, there is definitely a visible common trend in the behavior of the two data sets. The diversity is not surprising taking into account the fact that only one function has been applied to the images. The derivative-based as well as any other sharpness function is not meant as a stand alone measurement of the image aesthetics. Such a function could be used within an aesthetics measurement system, which consists of a number of components, including pattern recognition techniques [3], [28]. In our experiment for the photos with the highest scores, the values of the gradient-based sharpness function do not go that high. This can be explained by the fact that the photos have gained the high scores not because of their general properties, but because of compositional details attractive for a human.

B. A common setting

Usually after a photoshoot photographers and picture editors must review a large collection of images to select the strongest ones. This is a difficult and time consuming task. By means of computational aesthetics this manual operation could become semi-automated. In this section we describe a numerical experiment with the photographs recorded within one photoshoot.

In total 138 photos are taken with the digital photocamera Hasselblad. In order to perform the experiments the original high resolution photos are changed to grayscale and decreased to the size 400×300 pixels. The samples of some of the images from the series are shown in the upper row of Figure 7. For each of the photos, derivative-based sharpness function (15), variance-based sharpness function (21) and histogram-based sharpness function (22) are computed. Figures 8(a)-8(c) show the results of these computations. Each of the computed functions has a pick in the middle, around the image with the number 64. The peaks indicate the image that could be desirable as the experimental output.

For the derivative-based sharpness functions the experiments have been also performed for different values of the blur parameter α . Figure 9 shows results of these computations. For the larger values of α the function is less noisy, but the peak is less established. However, the position of the



(a) Landscape photograph.



(b) The Sobel operator, used as energy map.

(c) $S = 0.5$ (d) $S = 0.7$ (e) $S = 0.9$

Fig. 10. Landscape image sublimated based on use of Sobel operator as energy function.

peak does not change.

VII. IMAGE SUBLIMATION

In the previous section we demonstrate the application of sharpness functions for computational aesthetics. This might be useful for a number of visualization applications, for example generating scatterplots of images [32]. In [32], not only are numerical attributes of images plotted, but so too are the images themselves: “Typical information visualization involves first translating the world into numbers and then visualizing relations between these numbers. In contrast, media visualization involves translating a set of images into a new image which can reveal patterns in the set.” [32]

This technique has proven useful for visualizing diverse sets of images, the sort discussed earlier in section VI-A. At the same time, for sets of similar images, for example those discussed in section VI-B, it fails to show subtle differences. Instead, we note that sharpness functions provide a measure of importance not just of images, but also *within* images, and propose to exploit the spatial nature of sharpness analysis to visualize the most important regions in an image.

In [33], spatial analysis of an image is combined with seam-removal for automatic *Image Retargeting*, or changing the aspect ratio of an image. Different spatial analysis techniques are used as *energy maps* to select seams (contiguous paths through an image) of minimal energy that may be removed. If the image is first upsampled and then returned to its original size with seam removal, important regions of the image are enlarged to comparatively greater size (see Figure 10). This method is suggested in [33] as “content amplification.” In the context of computational aesthetics, we call this method *sublimation* and trivially formalize it by parameterizing the transformation with a *sublimation factor* S , such that a percentage of relatively-uninteresting pixels equal to S are removed from the image.

Experimental results are shown in Figure 11, where a series of sharpness-function-guided sublimateations of related photographs are presented in comparison to traditionally downsampled images. The caricatures are generated using sublimation of the most aesthetically pleasing regions of images, which are determined with the help of our sharpness function (Equation 17). The sharpness function is used directly as an energy function in the open source Liquid Rescale Library [34].

The sublimation transformation itself exhibits strong aesthetic qualities, an attribute noted but not explored here.

VIII. DISCUSSION AND FUTURE RECOMMENDATIONS

In this paper we have suggested a number of sharpness functions that could be used for the purpose of computational aesthetics and image sublimation. The extensive study of the sharpness functions could provide improvement in the variety of fields, such as for instance image enhancement [29] and image retrieval [35], [36].

The sharpness functions are not meant as a stand-alone instrument for computational aesthetics. However, they could be a useful extension for the aesthetics measurement systems, such as [3], [28]. In future a wider range of sharpness functions could be applied for the same purpose, for instance, autocorrelation-based sharpness functions [17], [24], [37] or Fourier-transform based sharpness functions [38]. The later is often replaced nowadays with the wavelet-based approaches [29], [39].

Only image derivatives of the first order [4], [21] or the second order [9], [8] have been applied so far as a sharpness function. The application of the derivatives of the higher order ($n > 2$ in (9)) could be a topic of the future research and might lead to the improvements.

For the derivative-based sharpness function we have chosen the L^2 -norm, because it is the most practically used

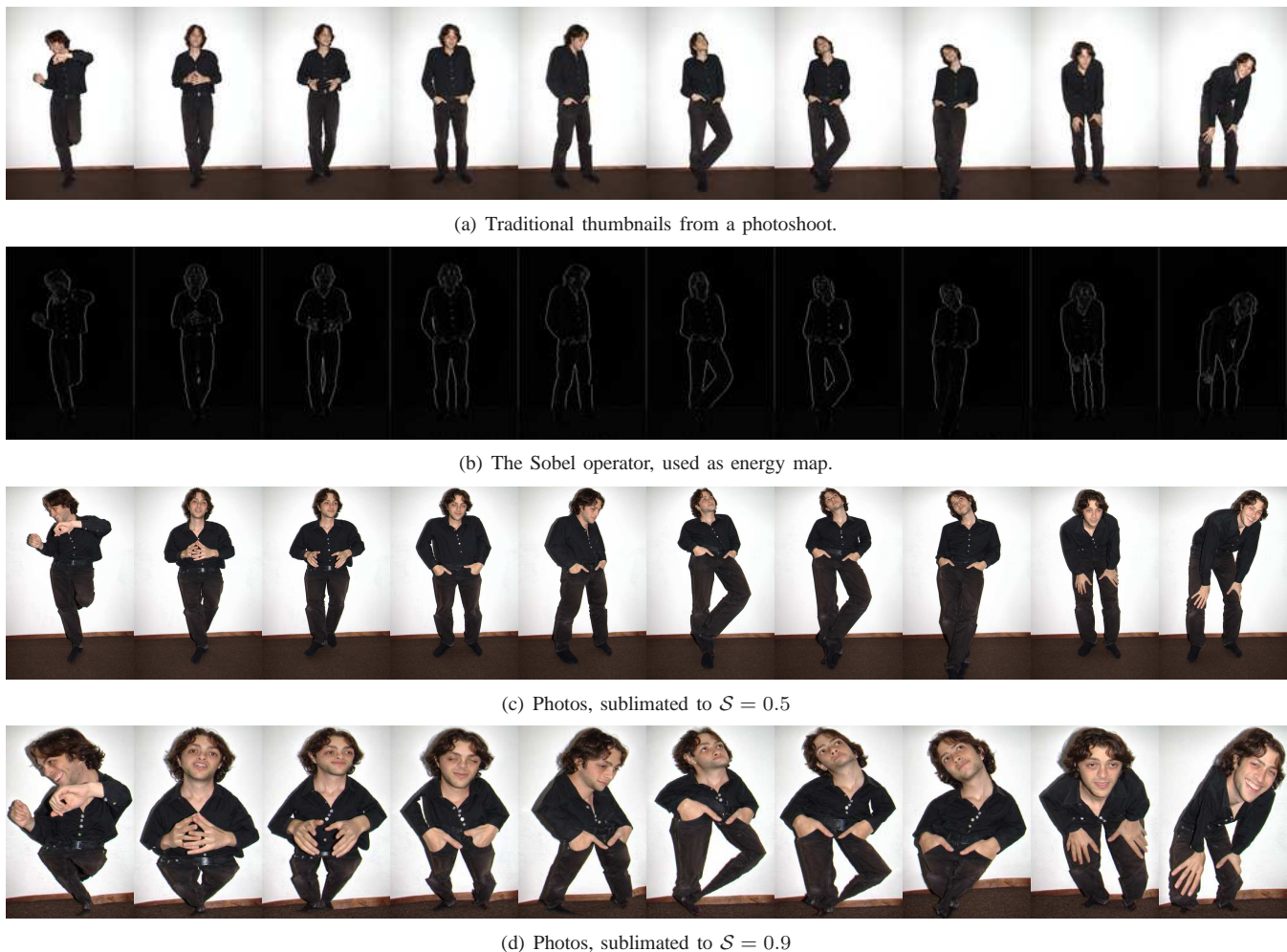


Fig. 11. Set of experimental images sublimated based on use of Sobel operator as energy function.

norm with a lot of proven mathematical properties. This simplifies the analysis [5]. For instance a relatively trivial proof of the fact that derivative-based sharpness function reaches its maximum at $\sigma = 0$ for the L^2 -norm case could be complicated in the case of L^1 -norm or the general L^p -norm. In practice the L^1 -norm derivative-based sharpness function is used as well [25], [19]. Our observations could be probably generalized for the L^p -norm case.

We have also shown the use of sharpness functions to *sublimate* images. If computational aesthetics can determine “how soothing a picture is to the eyes” [3], its analysis may also help us condense images to their most sublime. In fact, the sublimation technique is applicable to any feature extraction that is spatial, and future work could explore combinations of different features into energy maps. One fault is that the current usage of the sharpness function makes sublimation sensitive to high-detail areas that may be common to many images; techniques from automatic caricature generation like “Exaggerating the Difference from the Mean” [40] may allow for more robust condensations. Finally, user-controlled sublimation may be a useful addition to photo navigation and selection interfaces.

ACKNOWLEDGMENT

The image of the photocamera used in Figure 1 has been downloaded from the Free Photoshop PSD file download

www.psdgraphics.com. The photo shown in Figure 5 is taken by Olga Ganzha.

We would like to acknowledge Lynsey Sims (model), Soraya Hoetmer, Kinmei Wong, Lourdes Ortiz Pereira for assistance with gathering the experimental data, described in Subsection VI-B.

REFERENCES

- [1] D. Joshi, R. Datta, Q. Luong, E. Fedorovskaya, J. Wang, J. Li, and J. Luo, “Aesthetics and emotions in images: A computational perspective,” *IEEE Signal Processing Magazine*, vol. 28, no. 5, pp. 94–115, 2011.
- [2] P. Tinio, H. Leder, and M. Strasser, “Image quality and aesthetic judgment of photographs: Contrast, sharpness and grain teased apart and put together,” *Psychology of Aesthetics, Creativity, and the Arts*, vol. 5, no. 2, pp. 165–176, 2010.
- [3] R. Datta, D. Joshi, J. Li, and W. J.Z., “Studying aesthetics in photographic images using a computational approach,” in *Lecture Notes in Computer Science, Proceedings of the European Conference on Computer Vision, Part III*, vol. 3953, Graz, Austria, 2006, pp. 288–301.
- [4] M. Rudnaya, R. Mattheij, J. Maubach, and H. ter Morsche, “Gradient-based sharpness function,” in *Lecture Notes in Engineering and Computer Science: Proceedings of The World Congress on Engineering 2011, WCE*, London, UK, 6-8 July 2011, pp. 301–306.
- [5] M. Rudnaya, H. ter Morsche, J. Maubach, and R. Mattheij, “A derivative-based fast autofocus method in electron microscopy,” *Journal of Mathematical Imaging and Vision*, vol. accepted, 2011.
- [6] V. Vijaykumar, P. Vanathi, and P. Kanagasabapathy, “Fast and efficient algorithm to remove gaussian noise in digital images,” *IAENG International Journal of Computer Science*, vol. 37, no. 1, 2010.

- [7] S. Morigi, L. Reichel, F. Sgallari, and A. Shyshkov, "Cascadic multi-resolution methods for image deblurring," *SIAM J. Imaging Sci.*, vol. 1, no. 1, pp. 51–74, 2007.
- [8] K. Kumar, M. Pisarenco, M. Rudnaya, V. Savcenko, and S. Srivastava, "Shape reconstruction techniques for optical sectioning of arbitrary objects," *Mathematics-in-Industry Case Studies J.*, vol. 3, pp. 19–36, 2011.
- [9] S. K. Nayar and Y. Nakagawa, "Shape from focus," *IEEE Trans. Pattern Anal. Mach. Intell.*, vol. 16, no. 8, pp. 824–831, 1994.
- [10] A. Carasso, D. Bright, and A. Vladar, "APEX method and real-time blind deconvolution of scanning electron microscopy imagery," *Opt. Eng.*, vol. 41, no. 10, pp. 2499–2514, 2002.
- [11] C. Johnson, "A method for characterizing electro-optical device modulation transfer function," *Photograph. Sci. Eng.*, vol. 14, no. 413–415, 1970.
- [12] d. V. Vriendt, "Fast computation of unbiased intensity derivatives in images using separable filters," *Int. J. Comp. Vis.*, vol. 13, no. 3, pp. 259–269, 1994.
- [13] L. Florack, B. t. Haar Romeny, J. Koenderink, and M. Viegerver, "Scale and differential structure of images," *Im. Vis. Comp.*, vol. 10, no. 6, pp. 376–388, 1992.
- [14] A. Erteza, "Sharpness index and its application to focus control," *Appl. Opt.*, vol. 15, no. 4, pp. 877–881, 1976.
- [15] E. Krotkov, "Focusing," *Int. J. Comput. Vis.*, vol. 1, pp. 223–237, 1987.
- [16] R. Muller and A. Buffington, "Real-time correction of atmospherically degraded telescope images through image sharpening," *J. Opt. Soc. Am.*, vol. 64, no. 9, pp. 1200–1210, 1974.
- [17] V. Hilsenstein, "Robust autofocus for automated microscopy imaging of fluorescently labelled bacteria," in *Proc. International Conference on Digital Image Computing: Techniques and Applications*, 2005.
- [18] M. Rudnaya, R. Mattheij, and J. Maubach, "Iterative autofocus algorithms for scanning electron microscopy," *Microscopy and Microanalysis*, vol. 15(Suppl 2), pp. 1108–1109, 2009.
- [19] M. Rudnaya, J. Maubach, and R. Mattheij, "Evaluating sharpness functions for automated scanning electron microscopy," *Journal of Microscopy*, vol. 240, pp. 38–49, 2010.
- [20] P. Van Bree, C. Van Lierop, and P. Van den Bosch, "Electron microscopy experiments concerning hysteresis in the magnetic lens system," in *Proc. IEEE Conference on Control Applications (CCA), Multi-Conference on Systems and Control*, Yokohama, Japan, 2010.
- [21] J. Brenner, B. Dew, J. Brian Horton, T. King, P. Neurath, and W. Selles, "An automated microscope for cytologic research a preliminary evaluation," *J. Histochem. Cytochem.*, vol. 24, no. 1, pp. 100–111, 1976.
- [22] R. Jarvis, "Focus optimization criteria for computer image processing," *Microscope*, vol. 24, pp. 163–180, 1976.
- [23] G. Ligthart and F. Groen, "A comparison of different autofocus algorithms," in *Proc. 6th Int. Joint Conf. on Pattern Recognition*, Munich, Germany, 1982, pp. 597–600.
- [24] D. Vollath, "Automatic focusing by correlative methods," *J. Microsc.*, vol. 147, pp. 279–288, Sep 1987.
- [25] A. Santos, C. De Solórzano, J. Vaquero, J. Peña, N. Malpica, and F. Del Pozo, "Evaluation of autofocus functions in molecular cytogenetic analysis," *J. Microsc.*, vol. 188, pp. 264–272, 1997.
- [26] S. Erasmus and K. Smith, "An automatic focusing and astigmatism correction system for the SEM and CTEM," *J. Microsc.*, vol. 127, no. 2, pp. 185–199, 1982.
- [27] M. Rudnaya, W. Van den Broek, R. Doornbos, R. Mattheij, and J. Maubach, "Autofocus and twofold astigmatism correction in HAADF-STEM," *Ultramicroscopy*, vol. 111, pp. 1043–1054, 2011.
- [28] S. Dhar, V. Ordóñez, and T. Berg, "High level describable attributes for predicting aesthetics and interestingness," in *IEEE Conference on Computer Vision and Pattern Recognition (CVPR)*, 2011.
- [29] A. R. M. Nair, R. Vrinthavani, and R. Tatavarti, "An alpha rooting based hybrid technique for image enhancement," *Engineering Letters*, vol. 19, no. 3, 2011.
- [30] B. Nys, I. Geuens, J. Naudts, R. Gijbels, W. Jacob, and P. Van Espen, "A convenient method for autofocus based on image information content," *J. of Computer-Assisted Microscopy*, vol. 2, no. 2, pp. 115–123, 1990.
- [31] R. Gonzalez, R. Woods, and S. Eddings, *Digital image processing using MATLAB*. Upper Saddle River: Pearson Prentice Hall, 2004.
- [32] L. Manovich, *Media Studies Futures*. Blackwell, forthcoming 2012, ch. Media Visualization: Visual Techniques for Exploring Large Media Collections, <http://lab.softwarestudies.com/2009/06/publications.html>.
- [33] S. Avidan and A. Shamir, "Seam carving for content-aware image resizing," *ACM Transactions on Graphics*, vol. 26, no. 3, 2007.
- [34] C. Baldassi, "Free software liquid rescale library," <http://liblqr.wikidot.com/>.
- [35] N. Zhang, K. Man, T. Yu, and C. Lei, "Text and content based image retrieval via locality sensitive hashing," *Engineering Letters*, vol. 19, no. 3, 2011.
- [36] R. Perez-Aguila, "Automatic segmentation and classification of computed tomography brain images: An approach using one-dimensional kohonen networks," *IAENG International Journal of Computer Science*, vol. 37, 2010.
- [37] M. Rudnaya, R. Mattheij, J. Maubach, and H. terMorsche, "Autocorrelation-based sharpness functions," in *Proc. 3rd IEEE International Conference on Signal Processing Systems*, Yantai, China, 2011.
- [38] M. Rudnaya, R. Mattheij, J. Maubach, and H. ter Morsche, "Orientation identification of the power spectrum," *Optical Engineering*, vol. 50, no. 103201, 2011.
- [39] G. Yang and B. Nelson, "Wavelet-based autofocusing and unsupervised segmentation of microscopic images," in *Proc. of the Intl. Conference on Intelligent Robots and Systems*, 2003.
- [40] Z. Mo, J. P. Lewis, and U. Neumann, "Improved automatic caricature by feature normalization and exaggeration," in *ACM SIGGRAPH 2004 Sketches*, ser. SIGGRAPH '04. New York, NY, USA: ACM, 2004, pp. 57–. [Online]. Available: <http://doi.acm.org/10.1145/1186223.1186294>